Synthesis of Metal-Organic Frameworks Zinc (II) with Optimum Slow Pyrolysis Process for Conductivity Performance

Wara Dyah Pita Rengga[1*], *Amelia* Fitri[2], *Sutikno* Madnasri[3], and *Fauzi* Syahputra[4]

[1,2,4]Chemical Engineering Department. Universitas Negeri Semarang, 50229 Semarang, Indonesia
[3]Physics Department. Universitas Negeri Semarang, 50229 Semarang, Indonesia

Abstract Metal-organic frameworks are one of the materials that currently have the potential as an anode material to replace graphite. It also has the advantages of large specific surface area, storage space and high gas absorption with high pore volume and good conductivity. The purpose of this study was to determine the optimum temperature for the synthesis of Metal-Organic Frameworks to obtain conductivity performance. Zinc nitrate hexahydrate and acetic acid were mixed in N, N-Dimthylformamide solvent at various temperatures of 250-650 ℃ for 4 hours with a slow pyrolysis process and proceeded with precipitation. Solid Metal-Organic Frameworks formed were characterized using Scanning Electron Microscopy, X-ray diffraction, Fourier Transform Infra-Red, and IV-Meter. The crystal form is nanocubes of a layered metal-organic framework of Zinc (II) that penetrates each other in a hexagonal shape. The crystal contains zinc oxide with hydroxyl and carboxylic functional groups. Metal-organic synthesis occurs at an optimum reaction temperature of 450 ℃, showing high conductivity, with the fastest current increase, reaching a current of 3.82E-08 A at a voltage of 0.05 V.

* Corresponding author: wdpitar@mail.unnes.ac.id

1. Introduction

In the present era, energy storage materials are highly demanded, especially batteries, which play a crucial and widespread role in supporting everyday activities [1]. Batteries have several core components, including the anode, cathode, separator, and nonaqueous electrolyte[2]. Batteries are classified into primary and secondary batteries. Among these types, secondary batteries are more widely used as they are more advantageous, rechargeable, and can be used repeatedly[3]. One particular type of secondary battery that is currently receiving special attention is the lithium-ion battery[4]. This type of battery possesses high energy density and storage capacity of up to 1000 mAh g^{-1}, excellent electrochemical reaction speed, and good conductivity properties[5]. However, lithium batteries consist of a graphite anode, a cathode made of oxide ($LiCoO_2$), and layers on the anode and cathode made of materials like polypropylene, polyethene, or laminates, separator, and nonaqueous electrolyte[6]. The anode of lithium batteries is known to have specific weaknesses[7]. Graphite is known to be expensive, scarce in nature, and has complexity during synthesis[8]. Additionally, a graphite-based anode can experience volume expansion (9-13%) during the process of lithium-ion intercalation, leading to a significant decrease in storage capacity over multiple charge-discharge cycles and reduced battery quality[9]. Ongoing exploration for new anode materials aims to discover environmentally friendly, easily accessible, and cost-effective alternatives[10].

Organic batteries are one of the energy storage materials due to their cost-effectiveness, ease of availability compared to conventional batteries, and environmental friendliness[11]. Organic batteries are not a new concept in energy storage, but they have the characteristic of electrodes composed of organic-based carbon anodes and cathodes[12].

Organic batteries can distribute energy rapidly and charge faster than non-organic materials[13]. Organic batteries have been extensively explored due to their similar properties to lithium batteries, making them more advantageous than inorganic batteries[14]. Organic batteries offer more excellent benefits than lithium batteries with graphite anodes, which are more expensive due to limited availability and environmental concerns[15]. One material that currently holds potential as a graphite replacement for anodes is Metal-Organic Frameworks (MOFs)[16]. Metal oxide materials like ZnO, CuO, Co_3O_4, and Fe_xO_y have been successfully fabricated to create MOF materials[17]. Therefore, this study employs Metal-Organic Frameworks (MOFs).

Metal-organic frameworks (MOFs) are three-dimensional (3D) microcrystalline structures composed of metal ions connected by organic linker materials[18]. MOFs exhibit advantages such as a large specific surface area, high gas storage and absorption capacity within their voluminous pores, and good conductivity properties[19]. Morphological and crystal size modifications of MOFs are crucial in synthesis methods as the shape and size of particles influence the functional properties of materials[20]. This study chose Zn for MOF synthesis due to its high gas absorption capacity, significant porosity, and suitability for further thermal treatment[21]. MOFs can function as anodes, and through subsequent heating, they can be transformed into MOF-derived carbon, representing a breakthrough in battery development[22]. MOF-derived carbon (MOF-DC) can be synthesized through high-temperature heating (pyrolysis), microwave irradiation, and solvothermal reactions[23].

Pyrolysis of MOFs holds promise in creating controllable porosity in porous carbons with large surface areas[23]. Pyrolysis is a thermochemical decomposition process in organic materials (biomass) under heating, converting the raw material into gaseous phase components[24]. Leng & and Huang (2018) added that pyrolysis can convert biomass into solid products like carbon. Pyrolysis is influenced by factors such as temperature, particle size of the raw material, catalyst, and retention time[25]. Utilizing pyrolysis in the

production of MOFs offers its advantages, resulting in MOFs with high intrinsic surface areas, open pore structures, and the ability to store energy with enhanced capacity[10].

Previous research has established that to employ MOFs as anodes in lithium batteries, critical requirements include porous carbon with a specific surface area exceeding 5000 m2/g, porosity with density <0.13 g/cm3, and high conductivity[10]. This notion is supported by other studies that state that MOFs possess a specific surface area of 7140 m2/g, extensive storage space, and high gas adsorption capabilities[19]. This study explores the influence of pyrolysis temperature on the synthesis process of MOFs as lithium battery anode materials to determine optimal conditions and characterize the resulting MOF materials.

2. Methods

2.1 MOF Synthesis

To prepare the MOF material, 1 g of zinc nitrate tetrahydrate ($Zn(NO_3)_2.6H_2O$) and 0.1 g of acetic acid were dissolved in 40 mL of DMF (N, N-Dimethylformamide). The mixture was heated at varying temperatures of 150°C, 250°C, 350°C, 450°C, 550°C, and 650°C for 4 hours to precipitate the MOF particles. The particles were filtered and soaked three times in DMF (N, N-Dimethylformamide) and three times in chloroform, each soaking lasting 8 hours. The particles were filtered one final time and heated uncovered at 200°C for 2 hours until the MOF precipitate was fully formed[10].

2.2 Material Characterization

The characterization of the MOF samples includes XRD, FTIR, and IV Meter analyses. X-ray diffraction (XRD) patterns were recorded using a PANalytical X'Pert spectrophotometer with COkα radiation, which was converted to CUkα radiation to obtain spectrum peaks aimed at determining the Full Width at Half Maximum (FWHM) and crystallinity of the MOF. It was followed by Fourier Transform Infrared (FTIR) analysis, involving the measurement of transmission spectra on a BRUKER-EQUI-NOX-55 IR spectrophotometer to identify organic and inorganic compounds. I-V (current-voltage) measurements were also conducted using the Nachriebe 100 I-V meter to generate data from current-voltage curves, allowing for conductivity determination. For imaging purposes, MOF samples were analyzed using a Scanning Electron Microscope (SEM) Phenom Pro X at magnifications up to 3 μm.

2.3 I-V Meter Measurements

I-V meter measurements of the MOF material were performed using the Nachriebe 100 I-V meter. The MOF material was dissolved in isopropyl alcohol and mixed with 5% by weight of ethylene glycol as a binder to coat onto a 1 cm2 ITO glass substrat[26]. After coating, the sample was air-dried at room temperature for 10 minutes. I-V scans were conducted from 0 to 10 V with a scanning rate of 5 mV/s.

3. Results and Discussion

3.1 SEM Results

The surface structure of MOF5 is depicted in Figure 1. MOF5, based on zinc nitrate, forms a nanostructure with circular patterns and fibre-like accents enveloping it. In this phase, the

carbon element's distinct structure is not yet visible, as this study utilized a maximum temperature of 650°C to prevent the volatilization of zinc. It corresponds to previous research[27], which demonstrated that the formed MOF structure resembles nanorods with a diameter of around 100 nm and a width of approximately 1 µm.

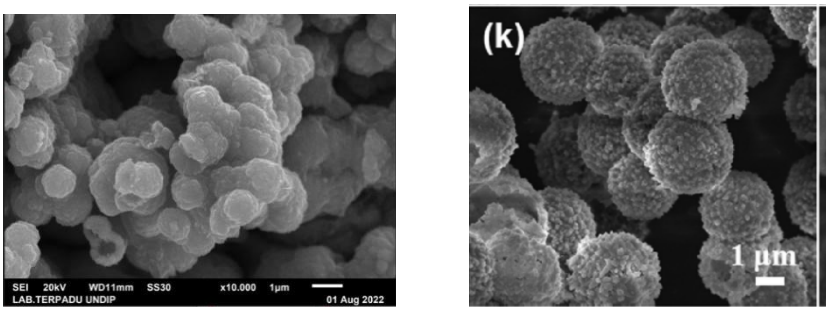

Figure 1. (a) SEM Image of MOF5 (Source: Research Results), (b) SEM Image of MOF Source: (Xu et al., 2018)

3.2 XRD Analysis

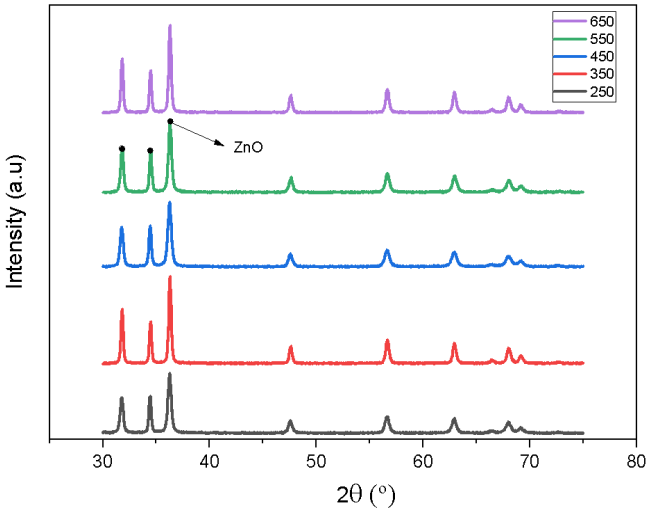

Figure 2. XRD Graph of MOF5 at heating temperature 250ºC, 350ºC, 450ºC, 550 ºC and 650ºC

Figure 2 illustrates the XRD patterns of the MOF5 sample at different temperatures. The results show a plot of the MOF5 crystallinity with a 100°C interval. Distinct diffraction peaks are observed on the graph, indicating that the tested sample falls within the crystalline category. The formed diffraction peaks correspond to the crystalline structure of ZnO and are found at angles 2θ 31.7°, 34.4°, and 36.2° with codes (100), (002), and (101), respectively, consistent with the crystal form of ZnO[28]. The observed peaks in the tested sample align with a previous study by Yang et al. (2019) at temperatures of 250-650°C, where peaks were found at angles 2θ of 31.8°, 34.4°, 36.2°, 47.5°, 56.6°, 62.8°, 66.4°, 68.0°, and 69.1°, indicating the crystal form of wurtzite hexagonal (JCPDS card No.36-1451).

Furthermore, the Full Width Half Maximum (FWHM) value is obtained, representing the breadth of the maximum peak. FWHM determines the size of the formed crystals; a higher FWHM value indicates a smaller particle size[29]. A previous study by Puspitasari (2019) stated that temperature influences the magnitude of crystal size[30].

Table 1. The Value of FWHM *(Full Width Half Maximum)*

SUHU (°C)	FWHM (radian)
250	0,5086
350	0,5592
450	0,6256
550	0,6265
650	0,3547

The tested samples revealed the smallest crystal size around temperatures of 450 - 550°C, with the most significant average FWHM values being 0.6256 and 0.6265, respectively, as shown in Table 4.1. It indicates that the crystals are the smallest at these temperatures. Smaller crystal sizes lead to larger surface areas, which can store more significant amounts of energy[10]. This phenomenon is attributed to the pyrolysis process employed in the fabrication of MOF5.

3.3 FTIR Analysis

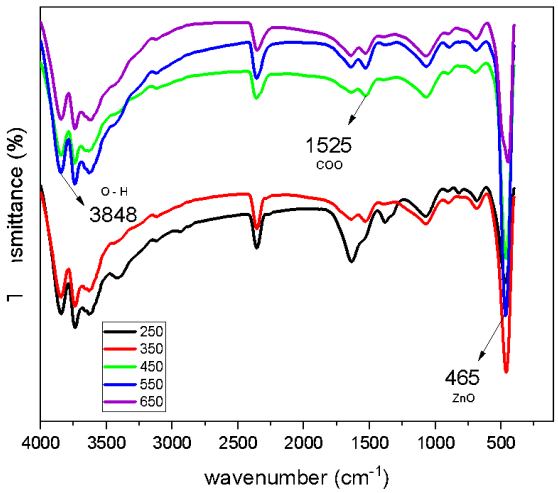

Figure 3. FTIR Spectra Graph of MOF5 at Heating Temperatures of 250°C, 350°C, 450°C, 550°C, and 650°C (Source: Research Findings)

Figure 3. (a) illustrates the outcomes of the conducted research. The graph presents the FTIR spectrum aimed at determining the functional groups of MOF5 and the reaction between Zn(NO3)2 ·6H2O (zinc nitrate hexahydrate) and CH3COOH (acetic acid), resulting in the formation of zinc acetate compounds with an octahedral structure[14]

Samples at 450 - 550°C peak at a wavenumber of 3789 cm-1, indicating the presence of hydroxyl groups (O-H). An absorption peak at 465 cm-1 also signifies the MOF structure's Zn-O functional group. A spectrum is also observed at a wavenumber of 1525 cm-1, suggesting the presence of carboxylate groups (C-O) originating from acetic acid.

The FTIR testing results at various temperatures, including 250°C, 350°C, 450°C, 550°C, and 650°C, demonstrate that the temperature range of around 450 - 550°C is the optimum temperature. This is because the highest peak appears in this range compared to other samples, as seen in Figure 4. The magnification of each sample's peak height is displayed, along with numerous broken lines. Furthermore, no evidence of damage to the MOF5 structure at this temperature confirms it as the most optimal condition[31].

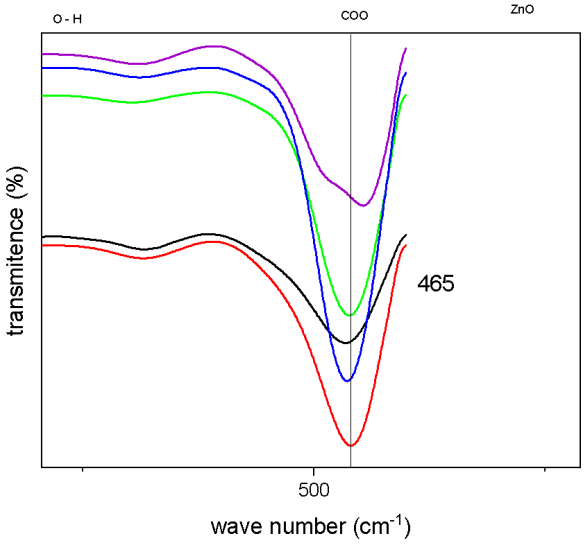

Figure 4. FTIR magnification at wavenumber 465cm^{-1}

Other hydroxyl groups, such as O-H stretch, can be found at wavenumbers >3550 cm^{-1}[32]. Furthermore, functional groups such as C-O can also be found at wavenumbers around 1300-1600 cm^{-1} [33]. Overall, the test results have identified functional groups consistent with previous research conducted by [34].

Table 2. FTIR test resultf of MOF5

Gugus Ikatan	*Wave number* (cm^{-1})
Zn-O	465
O-H *stretch*	3848
C-O	1525

3.4 IV-Meter Results Analysis

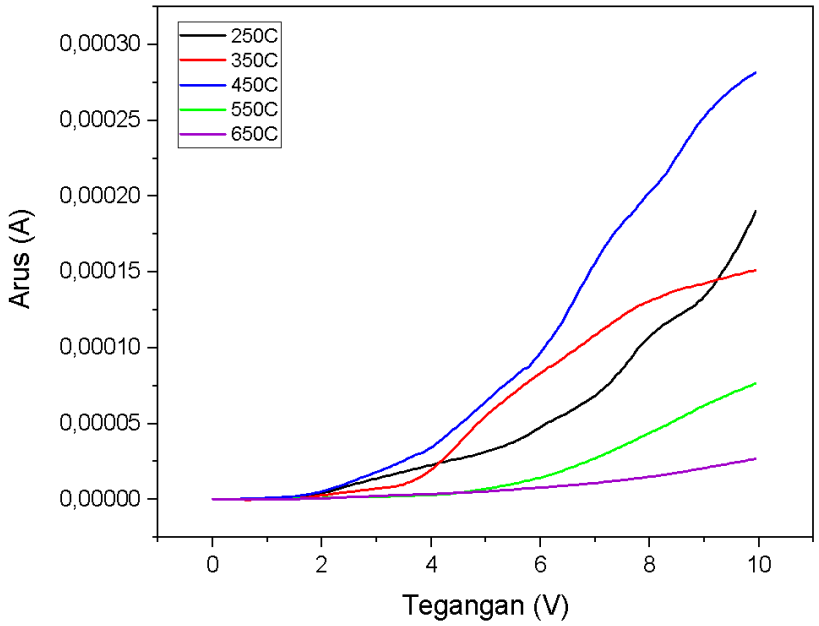

Figure 5. Exponential IV Graph of MOF5 at Temperature 250ºC, 350ºC. 450ºC, 550ºC, 650ºC

From the I-V meter measurements presented in Figure 8 above, it can be observed that the synthesized MOF5 material falls under the category of conductive materials capable of transmitting electricity. This is evident from the exponential graph formed, where such an exponential trend signifies the conductivity of a material when tested using an I-V meter[35]. Conversely, if a material produces a non-exponential graph, it falls within the category of semiconductive materials[36]. The purpose of the I-V meter testing is to determine whether the MOF5 material exhibits electrical conductivity or not. At a temperature of 450°C, the most rapid current increase occurs at a voltage of 0.05 V, with a current of 3.82E-08 A. The curve displays the highest slope at this point, indicating that this temperature exhibits the best conductivity among the tested temperatures, likely due to the higher carbon content formed[37]. Hence, the temperature of 450°C can be considered the optimum condition for obtaining MOF5 with high conductivity.

On the other hand, the shortest curve and slowest current increase, at a voltage of 0.2 V with a current of 6.68E-10 A, are observed at a temperature of 650°C. This indicates that at 650°C, the electrical conductivity is lowest. As the synthesis employs high temperatures, ion mobility is promoted, leading to potential disruptions in the formed crystal structure, consequently reducing the material's conductivity[38].

References

1. K. Zaghib *et al.*, "Lithium-Ion Cell Components and Their Effect on High-Power Battery Safety," in *Lithium-Ion Batteries: Advances and Applications*, Elsevier B.V., pp. 437–460 (2014)
2. Gels Handbook, "Section 2 - Batteries," in *Gels Handbook*, http://www.sciencedirect.com/science/article/pii/B978012394690450133X, 2001.
3. H. Qiao, Q. Wei, "Functional nanofibers in lithium-ion batteries," in *Functional Nanofibers and their Applications*, Elsevier, pp. 197–208 (2012)
4. S. Yonezawa, J. H. Kim, M. Takashima, "Electrochemical Behavior of Surface-Fluorinated Cathode Materials for Lithium Ion Battery," in *Advanced Fluoride-Based Materials for Energy Conversion*, Elsevier Inc., pp. 33–50 (2015)
5. S. Liu, X. Zhang, S. He, Y. Tang, J. Wang, B. Wang, S. Zhao, H. Su, Y. Ren, l. Zhang, J. Huang, Nano Energy, vol. **66**, 104159 (2019)
6. G. M. Gladysz, K. K. Chawla, "Applications," in *Voids in Materials*, Elsevier, pp. 131–156 (2015)
7. G. A. Kerchner, J. P. Wiaux, "Li-secondary battery: Special risks," in *Electrochemical Power Sources: Fundamentals, Systems, and Applications Li-Battery Safety*, Elsevier, pp. 455–505 (2018)
8. G. Kucinskis, G. Bajars, J. Kleperis, Journal of Power Sources, vol. **240**. pp. 66–79 (2013)
9. H. M. Lee and M. Ghovanloo, "Energy management integrated circuits for wireless power transmission," in *Implantable Biomedical Microsystems: Design Principles and Applications*, Elsevier Inc., pp. 87–111 (2015)
10. N. Ingersoll, Z. Karimi, D. Patel, R. Underwood, R. Warren, Electrochim Acta, vol. **297**, pp. 129–136 (2019)
11. J. Heiska, M. Nisula, and M. Karppinen, Journal of Materials Chemistry A, vol. **7**.32., pp. 18735–18758 (2019)
12. P. K. Panda, D. Singh, R. Ahuja, "Organic Batteries: the Route Toward Sustainable Electrical Energy Storage Technologies," in *Next-Generation Materials for Batteries*, AIP Publishing, pp. 1–22 (2021)
13. C. N. Gannett, L. Melecio-Zambrano, M. J. Theibault, B. M. Peterson, B. P. Fors, and H. D. Abruña, "Organic electrode materials for fast-rate, high-power battery applications," *Materials Reports: Energy*, vol. **1.1**. KeAi Communications Co., (2021)
14. S. Henke, "Metal-organic frameworks with additional flexible substituents – Modulating Responsiveness, Gas Sorption Selectivity & Network Topologies," *Dissertation*, (2011)
15. S. Bai, X. Liu, K. Zhu, S. Wu, H. Zhou, Nat Energy, vol. **1.7**, (2016)
16. K. Mohammadi, M. R. Movahhedy, and S. Khodaygan, J Aerosol Sci, vol. **135**, pp. 72–85 (2019)
17. J. Siregar, "PENGEMBANGAN MATERIAL NANO OKSIDA LOGAM DAN MODIFIKASINYA DENGAN CARBON NANOTUBE (CNT) SEBAGAI SENSOR GAS VOC," (2019)
18. Y. Qin, M. Hao, and Z. Li, "Metal–organic frameworks for photocatalysis," in *Interface Science and Technology*, Elsevier B.V., pp. 541–579 (2020)
19. Y. Lv, H. Yu, P. Xu, J. Xu, and X. Li, Sens Actuators B Chem, vol. **256**, pp. 639–647 (2018)

20. M. Nadjib, R. Ediati, Y. A. Sulistiyo, L. Nadifah, *Jurnal ILMU DASAR*, vol. **17.1**, p. 53, (2017)
21. Ata-ur-Rehman *et al.*, Arabian Journal of Chemistry, vol. **11.1**, pp. 26–33, (2018)
22. X. Li *et al.*, Advanced Energy Materials, vol. **8.23,** (2018)
23. A. K. Thakur, M. Majumder, S. P. Patole, K. Zaghib, M. V. Reddy, Materials Advances, vol. **2.8**, pp. 2457–2482 (2021)
24. K. Ridhuan, D. Irawan, R. Inthifawzi, Turbo : Jurnal Program Studi Teknik Mesin, vol. **8.1**, (2019)
25. S. Mutsengerere, C. H. Chihobo, D. Musademba, I. Nhapi, Renewable and Sustainable Energy Reviews, vol. **104**, pp. 328–336, (2019)
26. V. Chernikova, O. Shekhah, M. Eddaoudi, ACS Appl Mater Interfaces, vol. **8.31**, pp. 20459–20464, (2016)
27. X. Xu *et al.*, Adv Funct Mater, vol. **28.16**, (2018)
28. S. Yang *et al.*, Sci Rep, vol. **9.1**, (2019)
29. Novi Widyawati, "Analisis Pengaruh Heating Rate terhadap Tingkat Kristal dan Ukuran Butir Lapisan Tipis Bzt yang Ditumbuhkan dengan Metode Sol Gel," *Skripsi*, (2012)
30. D. Puspitasari, "Pengaruh suhu aktivasi terhadap karakteristik keratin sebagai anoda baterai ion lithium," *Thesis*, (2019)
31. S. Wang, X. Xie, W. Xia, J. Cui, S. Zhang, X. Du, High Temperature Materials and Processes, vol. **39.2020**, pp. 171–177, (2020)
32. H. Ghaedi, M. Ayoub, S. Sufian, B. Lal, Y. Uemura, Journal of Molecular Liquids, vol. **242**, pp. 395–403, (2017)
33. T. A. Mulyati, R. Ediati, A. Rosyidah, Indonesian Journal of Chemistry, vol. **15.2**, pp. 101–107 (2015)
34. K. S. R. and R. J. B. B. N. Iswarya, M.G. Kumar, Asian J Sci Res, pp. 1–6 (2012)
35. M.A. Fathoni, Jurnal Inovasi Fisika Indonesia, vol. **4.1**, (2015)
36. G. Pari *et al.*, Jurnal Penelitian Hasil Hutan, vol. **34.4**, pp. 309–322 (2016)
37. A. Imammuddin, S. Soeparman, W. Suprapto, A. Sonief, Jurnal Rekayasa Mesin, vol. **9.2**, pp. 135–141 (2018)
38. M. Indriati, R. Nuryanto, L. Suyati, Jurnal Kimia Sains dan Aplikasi, vol. **16.2**, pp. 46–49 (2013)